







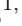




Nonlinearities in black hole ringdowns

Keefe Mitman ^{1,*} Macarena Lagos ^{2,†} Leo C. Stein ^{3,‡} Sizheng Ma,¹ Lam Hui,² Yanbei Chen,¹
 Nils Deppe ¹ François Hébert ¹ Lawrence E. Kidder ⁴ Jordan Moxon ¹
 Mark A. Scheel ¹ Saul A. Teukolsky ^{1,4} William Throwe ⁴ and Nils L. Vu ⁵

¹*Theoretical Astrophysics 350-17, California Institute of Technology, Pasadena, CA 91125, USA*

²*Department of Physics and Astronomy, Columbia University, New York, NY 10027, USA*

³*Department of Physics and Astronomy, University of Mississippi, University, Mississippi 38677, USA*

⁴*Cornell Center for Astrophysics and Planetary Science, Cornell University, Ithaca, New York 14853, USA*

⁵*Max Planck Institute for Gravitational Physics (Albert Einstein Institute), Am Mühlenberg 1, D-14476 Potsdam, Germany*

(Dated: August 17, 2022)

The gravitational wave strain emitted by a perturbed black hole (BH) ringing down is typically modeled analytically using first-order BH perturbation theory. In this Letter we show that second-order effects are necessary for modeling ringdowns from BH merger simulations. Focusing on the strain’s $(\ell, m) = (4, 4)$ angular harmonic, we show the presence of a quadratic effect across a range of binary BH mass ratios that agrees with theoretical expectations. We find that the quadratic $(4, 4)$ mode amplitude exhibits quadratic scaling with the fundamental $(2, 2)$ mode—its parent mode. The nonlinear mode’s amplitude is comparable to or even larger than that of the linear $(4, 4)$ modes. Therefore correctly modeling ringdown—improving mismatches by an order of magnitude—requires the inclusion of nonlinear effects.

Nonlinearity is responsible for the rich phenomenology of general relativity (GR). While many exact nonlinear solutions are known [1, 2], LIGO observables—gravitational waves (GWs) from merging binary black holes (BHs)—must be predicted by numerical relativity (NR). Analytic perturbation theory has an important role far from the merger: at early times, post-Newtonian (PN) theory; and at late times (ringdown), black hole perturbation theory [3–5], provided that the remnant asymptotes to a perturbed Kerr BH [6, 7]. PN theory has been pushed to high perturbative order [8], but the standard paradigm for modeling ringdown is only linear theory (see [9] for a review). It may then come as a surprise if linear theory can be used to model ringdown even at the peak of the strain [10–14], the most nonlinear phase of a BH merger.

The “magic” nature of the Kerr geometry [15] leads to a decoupled, separable wave equation for first-order perturbations (the Teukolsky equation [5]), schematically written as

$$\mathcal{T}\psi = \mathcal{S}, \quad (1)$$

where \mathcal{S} is a source term that vanishes for linear perturbations in vacuum, ψ is related to the first-order correction to the curvature scalar ψ_4 , and the linear differential Teukolsky operator \mathcal{T} depends on the dimensionless spin parameter $\chi \equiv |S|/M^2$ through the combination $a = |S|/M$ with S the BH spin angular momentum and M the BH mass (throughout we use geometric units $G = c = 1$). The causal Green’s function $\mathcal{G} \sim \mathcal{T}^{-1}$ has an infinite, but discrete set of complex frequency poles $\omega_{(\ell, m, n)}$ [16]. This makes GWs during ringdown well-described by a superposition of exponentially damped

sinusoids, called quasi-normal modes (QNMs). The real and imaginary parts of $\omega_{(\ell, m, n)}$ determine the QNM oscillation frequency and decay timescale, respectively. These modes are labeled by two angular harmonic numbers (ℓ, m) and an overtone number n . The combination $M\omega_{(\ell, m, n)}$ is entirely determined by χ .

To date, the linear QNM spectrum has been used to analyze current GW detections [17–19], forecast the future detectability of ringdown [20–22], and perform tests of gravity in the strong field regime [23, 24].

Since the sensitivity of GW detectors will increase in the coming years [25–28], there is the potential to observe nonlinear ringdown effects in high signal-to-noise ratio (SNR) events. A few previous works have shown that second-order perturbation effects can be identified in some NR simulations of binary BH mergers [29, 30]. In this Letter we show that quadratic QNMs—the damped sinusoids coming from second-order perturbation theory in GR—are a ubiquitous effect present in simulations across various binary mass ratios and remnant BH spins. In particular, for the angular harmonic $(\ell, m) = (4, 4)$, we find that the quadratic QNM amplitude exhibits the expected quadratic scaling relative to its parent—the fundamental $(2, 2)$ mode. The quadratic amplitude also has a value that is comparable to that of the linear $(4, 4)$ QNMs for every simulation considered, thus highlighting the need to include nonlinear effects in ringdown models of higher harmonics.

Quadratic QNMs.—Second-order perturbation theory has been studied for both Schwarzschild and Kerr BHs [31–41]. This involves the same Teukolsky operator as in Eq. (1) acting on the second-order curvature correction, and a complicated source \mathcal{S} that depends quadratically on the linear perturbations [39, 40, 42]. The second-order solution results from a rather involved integral of this source against the Green’s function \mathcal{G} [36, 41]. We only need to know that it is quadratic in the linear perturbation

* kmitman@caltech.edu

† m.lagos@columbia.edu

‡ lcstein@olemiss.edu

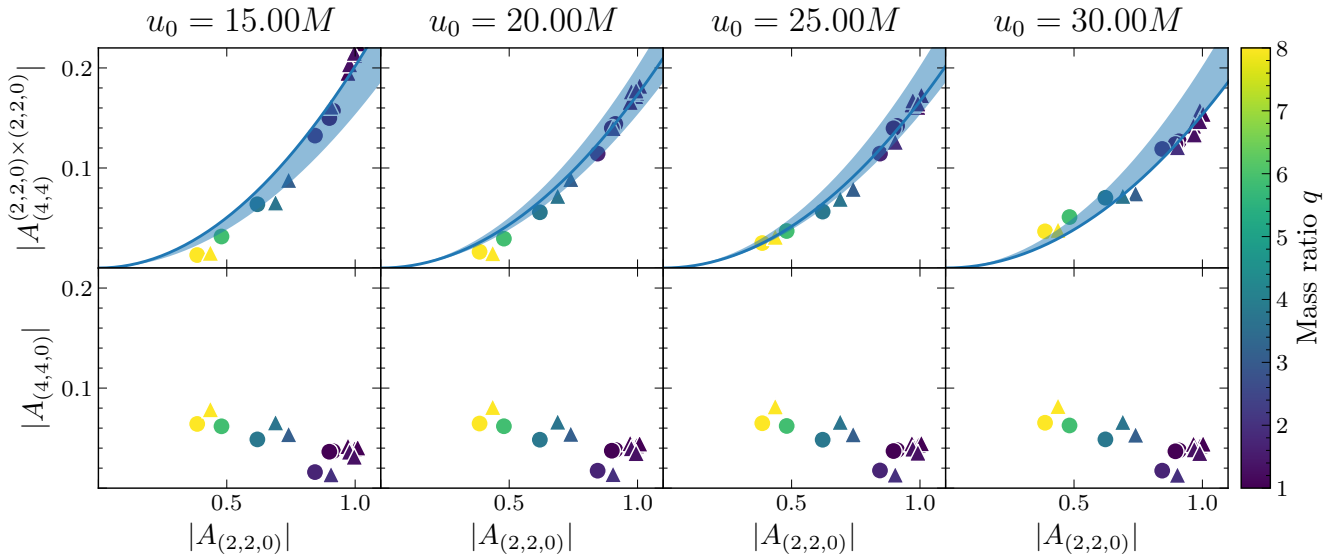


FIG. 1. Relationship between the peak amplitudes of the linear $(2, 2, 0)$ and the quadratic $(2, 2, 0) \times (2, 2, 0)$ QNMs (top panels) as well as the linear $(4, 4, 0)$ QNM (bottom panels), at different model start times u_0 . Colors show different mass ratios q , and circles and triangles denote systems with remnant dimensionless spin $\chi_f \approx 0.5$ and $\chi_f \approx 0.7$, respectively. Each blue curve is a pure quadratic fit with start time u_0 , and the shaded region brackets every one of the individual fits.

and that, after enough time, it is well-approximated by the quadratic QNMs.

The frequency spectrum of quadratic QNMs is distinct from the linear QNM spectrum. For each pair of linear QNM frequencies $\omega_{(\ell_1, m_1, n_1)}$ and $\omega_{(\ell_2, m_2, n_2)}$ (in either the left or right half complex plane), there will be a corresponding quadratic QNM frequency

$$\omega \equiv \omega_{(\ell_1, m_1, n_1)} + \omega_{(\ell_2, m_2, n_2)}. \quad (2)$$

As the linear $(2, \pm 2, 0)$ modes are most important, it is promising to investigate the quadratic QNMs they generate, which primarily appear in the $(\ell, m) = (4, \pm 4)$ modes [34, 35, 41]. The quadratic QNM coming from the $(2, 2)$ mode would have frequency $\omega_{(2,2,0) \times (2,2,0)} \equiv 2\omega_{(2,2,0)}$ and would decay faster than the linear fundamental mode $(4, 4, 0)$, but slower than the first linear overtone $(4, 4, 1)$, regardless of the BH spin [43].

The NR strain at future null infinity contains all of the angular information of the GW and is decomposed as

$$h^{\text{NR}}(u, \theta, \phi) \equiv \sum_{\ell=2}^{\infty} \sum_{|m| \leq \ell} h_{(\ell, m)}(u) {}_{-2}Y_{(\ell, m)}(\theta, \phi), \quad (3)$$

with u the Bondi time and ${}_{-2}Y_{(\ell, m)}$ the spin-weighted $s = -2$ spherical harmonics. We model this data with two different QNM ansätze, valid between times $u \in [u_0, u_f]$. The first model, which is typically used in the literature, involves purely linear QNMs,

$$h_{(\ell, m, N)}^{\text{model}, L}(u) = \sum_{n=0}^N A_{(\ell, m, n)} e^{-i\omega_{(\ell, m, n)}(u - u_{\text{peak}})}. \quad (4)$$

Here $A_{(\ell, m, n)}$ is the peak amplitude of the linear QNM with frequency $\omega_{(\ell, m, n)}$, N is the total number of overtones

considered in the model, and u_{peak} is the time at which the L^2 norm of the strain over the two-sphere achieves its maximum value (a proxy for the merger time), which we take to be $u_{\text{peak}} = 0$ without loss of generality. Note that here we have suppressed the spheroidal-spherical decomposition (which we include as in Eq. (6) of [44]).

We will use Eq. (4) to model both the $(2, 2)$ and $(4, 4)$ modes of the strain [45]. When modeling the $(2, 2)$ mode we use $N = 1$ and when modeling the $(4, 4)$ mode we use $N = 2$. While prior works have included more overtones in their models [10–14, 44], we restrict ourselves to no more than two overtones because we find that the amplitudes of higher overtones tend to vary with the model start time u_0 and hence are not very robust.

The novel QNM model, which includes second-order effects and highlights our main result, only changes how the $(4, 4)$ mode is described, compared to Eq. (4). It is given by

$$h_{(4,4)}^{\text{model}, Q}(u) = \sum_{n=0}^1 A_{(4,4, n)} e^{-i\omega_{(4,4, n)}(u - u_{\text{peak}})} + A_{(4,4)}^{(2,2,0) \times (2,2,0)} e^{-i\omega_{(2,2,0) \times (2,2,0)}(u - u_{\text{peak}})}, \quad (5)$$

where $A_{(4,4)}^{(2,2,0) \times (2,2,0)}$ is the peak amplitude of the quadratic QNM sourced by the linear $(2, 2, 0)$ QNM interacting with itself. Note that for the quadratic term we do not account for all of the angular structure, which requires the Green's function integral of the second-order source term. We emphasize that the two models $h_{(4,4,2)}^{\text{model}, L}(u)$ and $h_{(4,4)}^{\text{model}, Q}(u)$ contain the same number of free parameters.

In these ringdown models, we fix the QNM frequencies to the values predicted by GR in vacuum and fit the QNM

TABLE I. List of simulations used (ID is shorthand for SXS:BBH:ID from the SXS catalog [46] where the full list of binary parameters can be found) with their mass ratios q and dimensionless remnant spins χ_f . All of these binaries are non-precessing and are in quasi-circular orbits.

| | | | | | | | | | | |
|----------|------|------|------|------|------|------|----------|------|------|------|
| ID | 1502 | 1476 | 1506 | 1508 | 1474 | 1505 | 1504 | 1485 | 1486 | 1441 |
| q | 1.00 | 1.00 | 1.00 | 1.28 | 1.28 | 1.33 | 1.98 | 3.09 | 3.72 | 8.00 |
| χ_f | 0.73 | 0.68 | 0.71 | 0.73 | 0.73 | 0.71 | 0.71 | 0.68 | 0.70 | 0.72 |
| ID | 1500 | 1492 | 1465 | 1458 | 1438 | 1430 | ID | 0305 | | |
| q | 1.00 | 1.00 | 1.71 | 3.80 | 5.87 | 8.00 | q | 1.22 | | |
| χ_f | 0.53 | 0.48 | 0.48 | 0.47 | 0.47 | 0.50 | χ_f | 0.69 | | |

amplitudes to NR simulations, which cannot be predicted from first principles as they depend on the merger details. From the quadratic sourcing by the linear $(2, 2, 0)$ mode, we expect $A_{(4,4)}^{(2,2,0)\times(2,2,0)} \propto (A_{(2,2,0)})^2$. We will use this theoretical expectation as one main test to confirm the presence of quadratic QNMs. To perform this check we need a family of systems with different linear amplitudes, which is easily accomplished by varying the binary mass ratio $q \equiv m_1/m_2 \geq 1$.

The proportionality coefficient between $(A_{(2,2,0)})^2$ and $A_{(4,4)}^{(2,2,0)\times(2,2,0)}$ (which we expect to be order unity [36, 41]) comes from the spacetime dependence of the full quadratic source as well as the Green’s function. While in principle this can be computed, we use the fact that it should only depend on the dimensionless spin χ_f of the remnant BH.

We consider a family of 17 simulations (listed in Table I) of binary BH systems in the range $q \in [1, 8]$. To control the dependence on χ_f , 6 are in the range $\chi_f = 0.5 \pm 0.035$, and 10 have $\chi_f = 0.7 \pm 0.035$. The final simulation, SXS:BBH:0305, corresponds to GW150914 [47]. These simulations were produced using the Spectral Einstein Code (SpEC) and are available in the SXS Catalog [46, 48, 49]. For each simulation, the strain waveform has been extracted using Cauchy characteristic extraction (CCE) and has then been mapped to the superrest frame at $200M$ after u_{peak} [50–54] using the techniques presented in [54] and the code `scri` [55–58].

Quadratic Fitting.—In order to fit the ringdown models to the NR waveforms, using SciPy’s least squares implementation [59], we minimize the L^2 norm of the residual

$$\langle R, R \rangle \quad \text{for} \quad R \equiv h^{\text{NR}} - h^{\text{model}}, \quad (6)$$

where the inner product between waveforms a and b is

$$\langle a, b \rangle \equiv \int_{u_0}^{u_f} du \int_{S^2} d\Omega \overline{a(u, \theta, \phi)} b(u, \theta, \phi), \quad (7)$$

with $\overline{a(u, \theta, \phi)}$ being the complex conjugate of $a(u, \theta, \phi)$. We will fix $u_f = 100M$ and vary the value of u_0 . In Eq. (6), h^{model} is given by Eq. (4) with $N = 1$ for the $(2, 2)$ mode and Eq. (5) for the $(4, 4)$ mode by default, unless explicitly mentioned that we use the purely linear model, Eq. (4), with $N = 2$. We fix the frequencies and perform a spheroidal-to-spherical angular decomposition

of the linear terms in our QNM models using the open-source Python package `qnm` [60].

We show the main result of the fits in Fig. 1 for a range of initial times u_0 with which we find the best-fit amplitudes to be stable (shown later in Fig. 3). In the top panel, we see that $A_{(2,2,0)}$ and $A_{(4,4)}^{(2,2,0)\times(2,2,0)}$ clearly satisfy a quadratic relationship, illustrated by the shaded blue region that is obtained by combining the fitted quadratic curves for $u_0 \in [15M, 30M]$. In this region, we find the ratio $A_{(4,4)}^{(2,2,0)\times(2,2,0)} / A_{(2,2,0)}^2$ to range between 0.20 and 0.15 [61]. There is no noticeable difference in the quadratic relationship followed by the 0.7 and 0.5 spin families of waveforms, compared to the variations that are observed in the best-fit $A_{(4,4)}^{(2,2,0)\times(2,2,0)}$ due to the choice of the model start time u_0 .

We emphasize that this quadratic behavior is unique to the $A_{(4,4)}^{(2,2,0)\times(2,2,0)}$ mode, as can be seen in the bottom panel of Fig. 1, where we show the best-fit linear amplitude $A_{(4,4,0)}$ as a function of $A_{(2,2,0)}$. These two modes are not related quadratically (for more on their scaling with mass ratio, see [62]), which confirms the distinct physical origin of $A_{(4,4,0)}$ and $A_{(4,4)}^{(2,2,0)\times(2,2,0)}$. The best-fit amplitudes of $A_{(4,4,0)}$ and $A_{(2,2,0)}$ are nearly constants across these values of u_0 , which is why the four bottom figures look the same. A key result of Fig. 1 is that $A_{(4,4)}^{(2,2,0)\times(2,2,0)}$ is comparable to or larger (by a factor of ~ 4 in cases with $q \approx 1$) than $A_{(4,4,0)}$ at the time of the peak. Given that the exponential decay rates of $A_{(4,4)}^{(2,2,0)\times(2,2,0)}$ and $A_{(4,4,0)}$ for a BH with $\chi_f = 0.7$ are $\text{Im}[M\omega_{(2,2,0)\times(2,2,0)}] = -0.16$ and $\text{Im}[M\omega_{(4,4,0)}] = -0.08$, respectively, even beyond $10M$ after u_{peak} the quadratic mode will be larger than the linear mode for equal mass ratio binaries [63]. Thus, for large SNR events in which the $(4, 4)$ mode is detectable, the quadratic QNM could be measurable.

Comparisons.—Fig. 2 shows the GW150914 simulation (SXS:BBH:0305) and its fitting at $u_0 = 18M$, the time at which the residual in the $(4, 4)$ mode reaches its minimum. The top panel shows the waveform fit with the $(4, 4)$ quadratic model $h_{(4,4)}^{\text{model}, Q}$ as a function of time, where we find that it can fit rather well the amplitude and phase evolution of the numerical waveform at late times. The bottom panel shows the residual of the NR waveform with the linear and quadratic $(4, 4)$ QNM models, $h_{(4,4,2)}^{\text{model}, L}$ and $h_{(4,4)}^{\text{model}, Q}$, and a conservative estimate for the numerical error obtained by comparing the highest and second highest resolution simulations for SXS:BBH:0305. We see that even though the linear and quadratic $(4, 4)$ models have the same number of free parameters, the residual of $h_{(4,4)}^{\text{model}, Q}$ is nearly an order of magnitude better, which confirms the importance of including quadratic QNMs. Since, in general, the quadratic mode decays in time slower than the $(4, 4, 2)$ QNM, the quadratic model generally better describes the late time behavior of the waveform. In addition, the best-fit value of $A_{(4,4,0)}$ —which is the

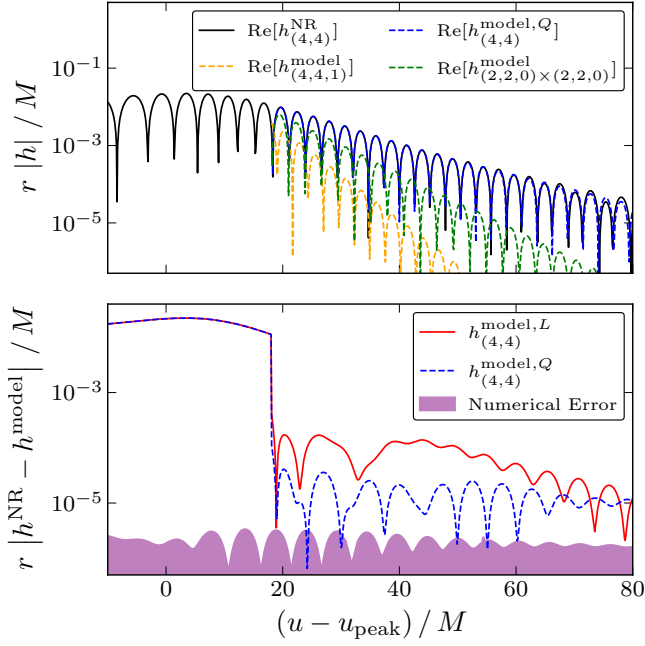


FIG. 2. Top panel: in black, the NR waveform for the SXS:BBH:0305 simulation and its comparison to the quadratic (4,4) QNM model (total in dashed blue, and individual QNMs in green and yellow) with start time $u_0 = 18M$. Bottom panel: residual in the (4,4) mode when using the linear (solid red) or the quadratic (dashed blue) (4,4) model. We also show a conservative estimate of the numerical error.

most important QNM in (4,4) at late times—differs in the linear and quadratic models, which causes the residuals to be rather different even beyond $u = 50M$ when we expect the overtones and quadratic mode to be sub-dominant.

In addition to the residuals, we quantify the goodness of fit by our models through the mismatch

$$\mathcal{M} = 1 - \text{Re} \left[\frac{\langle h^{\text{NR}} | h^{\text{model}} \rangle}{\sqrt{\langle h^{\text{NR}} | h^{\text{NR}} \rangle \langle h^{\text{model}} | h^{\text{model}} \rangle}} \right]. \quad (8)$$

The top panel of Fig. 3 shows the mismatch in the (4,4) mode between the NR waveform and the QNM model as a function of u_0 . The red and black lines show the results for the SXS:BBH:0305 simulation when the (4,4) mode was modeled with $h_{(4,4,2)}^{\text{model},L}$ and $h_{(4,4)}^{\text{model},Q}$, respectively. As a reference, we also show the numerical error calculated for SXS:BBH:0305 [64]. We see that the numerical error is below the fitted model mismatches for $u_0 \lesssim 40M$, but causes the mismatch to worsen at late times. We also see that the linear model performs worse than the quadratic model for any u_0 , confirming that the residual difference shown in the bottom panel of Fig. 2 was not a coincidence of the particular fitting time chosen there. At times $u_0 \approx 20M$, we see that the mismatch is about one order of magnitude better in the quadratic model. We find similar results for all of the simulations analyzed in this Letter [65] (grey thin curves show the mismatch of the $h_{(4,4)}^{\text{model},Q}$ in those simulations), although the mismatch difference

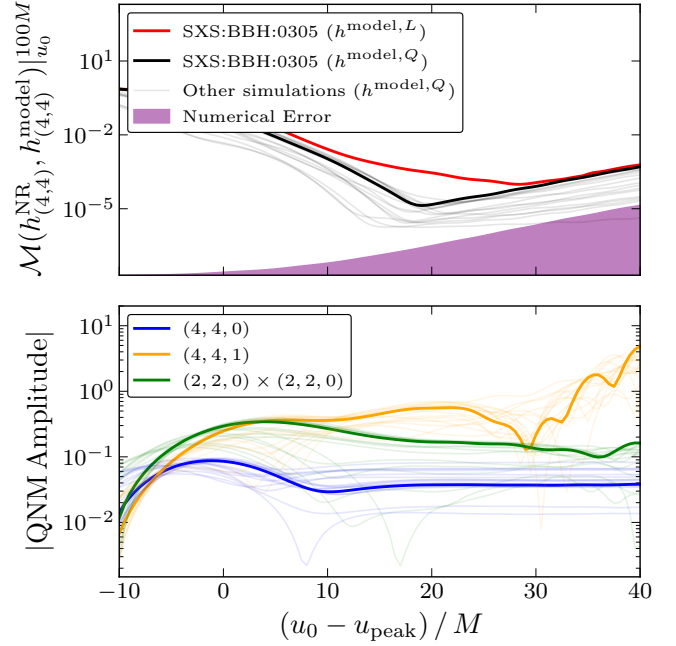


FIG. 3. Top panel: mismatch in the (4,4) mode for SXS:BBH:0305 as well as every other simulation examined, and a comparison to the numerical error floor. Bottom panel: amplitudes of the three QNM terms in the quadratic (4,4) QNM model as a function of the model start time u_0 .

becomes more modest for simulations with $q \approx 8$. When comparing the mismatches to the error, we find that in some simulations they start reaching the numerical error floor at around $u_0 \approx 30M$, which is why we take $u_0 \leq 30M$ in our fits. It is also beyond $u_0 \approx 30M$ that we see no considerable differences between the linear and quadratic model mismatches due to the high numerical error relative to the numerical strain’s amplitude.

In the bottom panel of Fig. 3 we show the best-fit amplitudes of the QNMs in the (4,4) mode as functions of u_0 . We show the results for SXS:BBH:0305 (thick lines) as well as the rest of the simulations (thin lines). We see that at $u_0 \gtrsim 10M$ the amplitude of $A_{(4,4,0)}$ is extremely stable, but the faster the additional QNM decays, the more variations that are seen. Nevertheless, the $A_{(4,4)}^{(2,2,0) \times (2,2,0)}$ exhibits only $\sim 20\%$ variations for $u_0 \in [15M, 30M]$, whereas $A_{(4,4,1)}$ varies by $\sim 70\%$ in the same range. Before and near $u_0 \approx 10M$ every amplitude shows considerable variations, which is why we use $u_0 \geq 15M$ in this Letter. This suggests a need to improve the QNM model, either by including more overtones as in [10], modifying the time dependence of the linear [66] and quadratic terms, or considering more nonlinear effects.

Finally we check which frequency is preferred by the (4,4) mode of the numerical strain. For this, we fix two frequencies to be the linear $\omega_{(4,4,0)}$ and $\omega_{(4,4,1)}$ frequencies, and keep one frequency free. We vary the frequency of that third term and fit every amplitude to minimize the residual in Eq. (6). Fig. 4 shows contours of the

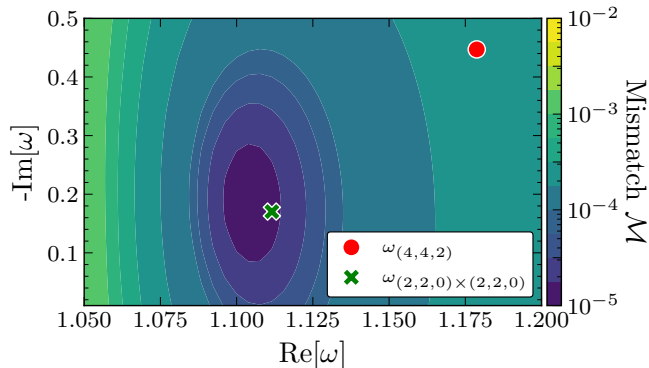


FIG. 4. Contour plot of the mismatch between the SXS:BBH:0305 waveform and a (4,4) model with three QNMs, in which two frequencies are fixed to the GR predictions of the linear (4,4,0) and (4,4,1) QNMs, but the third is varied. The start time of the model is taken to be $u_0 = 18M$.

mismatch over the real and imaginary parts of the unknown frequency for the SXS:BBH:0305 simulation using $u_0 = 18M$. We confirm that the data clearly prefers the frequency $\omega_{(2,2,0) \times (2,2,0)} = 2\omega_{(2,2,0)}$ over $\omega_{(4,4,2)}$.

Conclusions.—We have shown that second-order effects are present in the ringdown phase of binary BH mergers for a wide range of mass ratios, matching theoretical expectations and helping improve ringdown modeling at late times. We analyzed 17 NR simulations and in every one of them we found that, in the $(\ell, m) = (4, 4)$ mode, the quadratic QNM analyzed has a peak amplitude that is comparable to or larger than the $(\ell, m, n) = (4, 4, 0)$ fundamental linear QNM. Due to the relatively slow decay of this quadratic QNM, we find that for nearly equal-mass systems this QNM will be larger than the linear fundamental mode even $10M$ after u_{peak} .

These results highlight that we will be able to observe this nonlinear effect in future high SNR GW events with a detectable (4,4) harmonic. A quantitative analysis, and a generalization to other harmonics, will be performed in the future to assess in detail the detectability of quadratic QNMs for current GW detectors at design sensitivity as well as next-generation GW detectors.

The confirmation of quadratic QNMs opens new possibilities for more generally understanding the role of nonlinearities in the ringdown of perturbed black holes. It is now clear that we can readily improve the basic linear models that have been used previously in theoretical and observational ringdown analyses. Quadratic QNMs provide new opportunities to maximize the science return of GW detections, by increasing the likelihood of detecting multiple QNM frequencies. One of these key science goals is performing high-precision consistency tests of GR with GW observations. Fulfilling this goal requires a correct ringdown model, which incorporates the nonlinear effects that we have shown to be robustly present.

Note Added.—While preparing this Letter, we learned that Cheung *et al.* conducted a similar study, whose results agree with ours [67].

Acknowledgments.—We thank Max Isi and the Flatiron Institute for fostering discourse, and Vishal Baibhav, Emanuele Berti, Mark Cheung, Matt Giesler, Scott Hughes, and Max Isi for valuable conversations. Computations for this work were performed with the Wheeler cluster at Caltech. This work was supported in part by the Sherman Fairchild Foundation and by NSF Grants No. PHY-2011961, No. PHY-2011968, and No. OAC-1931266 at Caltech, as well as NSF Grants No. PHY-1912081, No. PHY-2207342, and No. OAC-1931280 at Cornell. The work of L.C.S. was partially supported by NSF CAREER Award PHY-2047382. M.L. was funded by the Innovative Theoretical Cosmology Fellowship at Columbia University. L.H. was funded by the DOE DE-SC0011941 and a Simons Fellowship in Theoretical Physics. M.L. and L.C.S. thank the Benasque Science Center and the organizers of the 2022 workshop “New frontiers in strong gravity,” where some of this work was performed; and M.L. acknowledges NSF Grant No. PHY-1759835 for supporting travel to this workshop.

-
- [1] H. Stephani, D. Kramer, M. A. H. MacCallum, C. Hoense-laers, and E. Herlt, *Exact solutions of Einstein's field equations*, Cambridge Monographs on Mathematical Physics (Cambridge Univ. Press, Cambridge, 2003).
 - [2] J. B. Griffiths and J. Podolsky, *Exact Space-Times in Einstein's General Relativity*, Cambridge Monographs on Mathematical Physics (Cambridge University Press, Cambridge, 2009).
 - [3] T. Regge and J. A. Wheeler, Stability of a Schwarzschild singularity, *Phys. Rev.* **108**, 1063 (1957).
 - [4] F. J. Zerilli, Gravitational field of a particle falling in a schwarzschild geometry analyzed in tensor harmonics, *Phys. Rev. D* **2**, 2141 (1970).
 - [5] S. A. Teukolsky, Perturbations of a rotating black hole. 1. Fundamental equations for gravitational electromagnetic and neutrino field perturbations, *Astrophys. J.* **185**, 635 (1973).
 - [6] R. Penrose, Gravitational collapse: The role of general relativity, *Riv. Nuovo Cim.* **1**, 252 (1969).
 - [7] P. T. Chrusciel, J. Lopes Costa, and M. Heusler, Stationary Black Holes: Uniqueness and Beyond, *Living Rev. Rel.* **15**, 7 (2012), arXiv:1205.6112 [gr-qc].
 - [8] L. Blanchet, Gravitational Radiation from Post-Newtonian Sources and Inspiralling Compact Binaries, *Living Rev. Rel.* **17**, 2 (2014), arXiv:1310.1528 [gr-qc].
 - [9] E. Berti, V. Cardoso, and A. O. Starinets, Quasinormal modes of black holes and black branes, *Class. Quant. Grav.* **26**, 163001 (2009), arXiv:0905.2975 [gr-qc].
 - [10] M. Giesler, M. Isi, M. A. Scheel, and S. Teukolsky, Black Hole Ringdown: The Importance of Overtones, *Phys. Rev. X* **9**, 041060 (2019), arXiv:1903.08284 [gr-qc].
 - [11] S. Bhagwat, X. J. Forteza, P. Pani, and V. Ferrari, Ringdown overtones, black hole spectroscopy, and no-hair theorem tests, *Phys. Rev. D* **101**, 044033 (2020), arXiv:1910.08708 [gr-qc].
 - [12] G. B. Cook, Aspects of multimode Kerr ringdown fitting, *Phys. Rev. D* **102**, 024027 (2020), arXiv:2004.08347 [gr-qc].

- qc].
- [13] X. Jiménez Forteza, S. Bhagwat, P. Pani, and V. Ferrari, Spectroscopy of binary black hole ringdown using overtones and angular modes, *Phys. Rev. D* **102**, 044053 (2020), [arXiv:2005.03260 \[gr-qc\]](#).
- [14] A. Dhani, Importance of mirror modes in binary black hole ringdown waveform, *Phys. Rev. D* **103**, 104048 (2021), [arXiv:2010.08602 \[gr-qc\]](#).
- [15] S. A. Teukolsky, The Kerr Metric, *Class. Quant. Grav.* **32**, 124006 (2015), [arXiv:1410.2130 \[gr-qc\]](#).
- [16] For this study we focus only on prograde modes (in the sense described in [44]), and therefore omit the additional prograde/retrograde label \pm . The Green's function also has branch cuts, which lead to power-law tails [68], that we ignore here.
- [17] M. Isi, M. Giesler, W. M. Farr, M. A. Scheel, and S. A. Teukolsky, Testing the no-hair theorem with GW150914, *Phys. Rev. Lett.* **123**, 111102 (2019), [arXiv:1905.00869 \[gr-qc\]](#).
- [18] E. Finch and C. J. Moore, Searching for a Ringdown Overtone in GW150914, [arXiv:2205.07809 \[gr-qc\]](#).
- [19] R. Cotesta, G. Carullo, E. Berti, and V. Cardoso, On the detection of ringdown overtones in GW150914, [arXiv:2201.00822 \[gr-qc\]](#).
- [20] E. Berti, A. Sesana, E. Barausse, V. Cardoso, and K. Belczynski, Spectroscopy of Kerr black holes with Earth- and space-based interferometers, *Phys. Rev. Lett.* **117**, 101102 (2016), [arXiv:1605.09286 \[gr-qc\]](#).
- [21] I. Ota and C. Chirenti, Overtones or higher harmonics? Prospects for testing the no-hair theorem with gravitational wave detections, *Phys. Rev. D* **101**, 104005 (2020), [arXiv:1911.00440 \[gr-qc\]](#).
- [22] S. Bhagwat, C. Pacilio, E. Barausse, and P. Pani, Landscape of massive black-hole spectroscopy with LISA and the Einstein Telescope, *Phys. Rev. D* **105**, 124063 (2022), [arXiv:2201.00023 \[gr-qc\]](#).
- [23] E. Berti, K. Yagi, H. Yang, and N. Yunes, Extreme gravity tests with gravitational waves from compact binary coalescences: (II) ringdown, *General Relativity and Gravitation* **50**, 10.1007/s10714-018-2372-6 (2018), [1801.03587](#).
- [24] R. Abbott *et al.* (LIGO Scientific, VIRGO, KAGRA), Tests of General Relativity with GWTC-3, [arXiv:2112.06861 \[gr-qc\]](#).
- [25] B. P. Abbott *et al.* (KAGRA, LIGO Scientific, Virgo, VIRGO), Prospects for observing and localizing gravitational-wave transients with Advanced LIGO, Advanced Virgo and KAGRA, *Living Rev. Rel.* **21**, 3 (2018), [arXiv:1304.0670 \[gr-qc\]](#).
- [26] L. S. Team, LISA Science Requirement Document.
- [27] M. Maggiore *et al.*, Science Case for the Einstein Telescope, *JCAP* **03**, 050, [arXiv:1912.02622 \[astro-ph.CO\]](#).
- [28] M. Evans *et al.*, A Horizon Study for Cosmic Explorer: Science, Observatories, and Community, [arXiv:2109.09882 \[astro-ph.IM\]](#).
- [29] L. London, D. Shoemaker, and J. Healy, Modeling ringdown: Beyond the fundamental quasinormal modes, *Phys. Rev. D* **90**, 124032 (2014), [Erratum: *Phys. Rev. D* **94**, 069902 (2016)], [arXiv:1404.3197 \[gr-qc\]](#).
- [30] S. Ma, K. Mitman, L. Sun, N. Deppe, F. Hébert, L. E. Kidder, J. Moxon, W. Throwe, N. L. Vu, and Y. Chen, Collective filters: a new approach to analyze the gravitational-wave ringdown of binary black-hole mergers, [arXiv:2207.10870 \[gr-qc\]](#).
- [31] R. J. Gleiser, C. O. Nicasio, R. H. Price, and J. Pullin, Colliding black holes: How far can the close approximation go?, *Phys. Rev. Lett.* **77**, 4483 (1996), [arXiv:gr-qc/9609022](#).
- [32] R. J. Gleiser, C. O. Nicasio, R. H. Price, and J. Pullin, Second order perturbations of a Schwarzschild black hole, *Class. Quant. Grav.* **13**, L117 (1996), [arXiv:gr-qc/9510049](#).
- [33] R. J. Gleiser, C. O. Nicasio, R. H. Price, and J. Pullin, Gravitational radiation from Schwarzschild black holes: The Second order perturbation formalism, *Phys. Rept.* **325**, 41 (2000), [arXiv:gr-qc/9807077](#).
- [34] K. Ioka and H. Nakano, Second and higher-order quasinormal modes in binary black hole mergers, *Phys. Rev. D* **76**, 061503 (2007), [arXiv:0704.3467 \[astro-ph\]](#).
- [35] H. Nakano and K. Ioka, Second Order Quasi-Normal Mode of the Schwarzschild Black Hole, *Phys. Rev. D* **76**, 084007 (2007), [arXiv:0708.0450 \[gr-qc\]](#).
- [36] S. Okuzumi, K. Ioka, and M.-a. Sakagami, Possible Discovery of Nonlinear Tail and Quasinormal Modes in Black Hole Ringdown, *Phys. Rev. D* **77**, 124018 (2008), [arXiv:0803.0501 \[gr-qc\]](#).
- [37] D. Brizuela, J. M. Martín-García, and M. Tiglio, A Complete gauge-invariant formalism for arbitrary second-order perturbations of a Schwarzschild black hole, *Phys. Rev. D* **80**, 024021 (2009), [arXiv:0903.1134 \[gr-qc\]](#).
- [38] E. Pazos, D. Brizuela, J. M. Martín-García, and M. Tiglio, Mode coupling of Schwarzschild perturbations: Ringdown frequencies, *Phys. Rev. D* **82**, 104028 (2010), [arXiv:1009.4665 \[gr-qc\]](#).
- [39] J. L. Ripley, N. Loutrel, E. Giorgi, and F. Pretorius, Numerical computation of second order vacuum perturbations of Kerr black holes, *Phys. Rev. D* **103**, 104018 (2021), [arXiv:2010.00162 \[gr-qc\]](#).
- [40] N. Loutrel, J. L. Ripley, E. Giorgi, and F. Pretorius, Second Order Perturbations of Kerr Black Holes: Reconstruction of the Metric, *Phys. Rev. D* **103**, 104017 (2021), [arXiv:2008.11770 \[gr-qc\]](#).
- [41] M. Lagos and L. Hui, Generation and propagation of nonlinear quasi-normal modes of a Schwarzschild black hole, In prep..
- [42] M. Campanelli and C. O. Lousto, Second order gauge invariant gravitational perturbations of a Kerr black hole, *Phys. Rev. D* **59**, 124022 (1999), [arXiv:gr-qc/9811019](#).
- [43] The $(\ell, m, n) = (2, 2, 0)$ can excite other quadratic QNMs with frequency $\omega = \omega_{(2,2,0)} - \bar{\omega}_{(2,2,0)}$. These will instead be related to the memory effect, as they are non-oscillatory. From angular selection rules they will be most prominent in the $(2, 0)$ mode. While these effects could also prove interesting to study, they are much more well-understood than the quadratic QNMs in the $(4, 4)$ mode, so we reserve their examination for future work [44, 69].
- [44] L. Magaña Zertuche, K. Mitman, N. Khera, L. C. Stein, M. Boyle, N. Deppe, F. Hébert, D. A. B. Iozzo, L. E. Kidder, J. Moxon, H. P. Pfeiffer, M. A. Scheel, S. A. Teukolsky, W. Throwe, and N. Vu, High precision ringdown modeling: Multimode fits and BMS frames, *Physical Review D* **105**, 10.1103/physrevd.105.104015 (2022), [2110.15922](#).
- [45] This is because the binary black hole simulations that we consider are non-precessing and are in quasi-circular orbits, so the $m < 0$ modes can be recovered from the $m > 0$ modes via $h_{(\ell, m)} = (-1)^{\ell} \overline{h_{(\ell, -m)}}$.
- [46] M. Boyle *et al.*, The SXS Collaboration catalog of binary black hole simulations, *Class. Quant. Grav.* **36**, 195006 (2019), [arXiv:1904.04831 \[gr-qc\]](#).

- [47] B. P. Abbott *et al.* (LIGO Scientific, Virgo), GW150914: First results from the search for binary black hole coalescence with Advanced LIGO, *Phys. Rev. D* **93**, 122003 (2016), [arXiv:1602.03839 \[gr-qc\]](#).
- [48] <https://www.black-holes.org/code/SpEC.html>.
- [49] SXS Gravitational Waveform Database, <http://www.black-holes.org/waveforms>.
- [50] J. Moxon, M. A. Scheel, and S. A. Teukolsky, Improved Cauchy-characteristic evolution system for high-precision numerical relativity waveforms, *Phys. Rev. D* **102**, 044052 (2020), [arXiv:2007.01339 \[gr-qc\]](#).
- [51] J. Moxon, M. A. Scheel, S. A. Teukolsky, N. Deppe, N. Fischer, F. Hébert, L. E. Kidder, and W. Thrope, The SpECTRE Cauchy-characteristic evolution system for rapid, precise waveform extraction, [arXiv:2110.08635 \[gr-qc\]](#).
- [52] N. Deppe, W. Thrope, L. E. Kidder, N. L. Fischer, C. Armaza, G. S. Bonilla, F. Hébert, P. Kumar, G. Lovelace, J. Moxon, E. O’Shea, H. P. Pfeiffer, M. A. Scheel, S. A. Teukolsky, I. Anantpurkar, M. Boyle, F. Foucart, M. Giesler, D. A. B. Iozzo, I. Legred, D. Li, A. Macedo, D. Melchor, M. Morales, T. Ramirez, H. R. Rüter, J. Sanchez, S. Thomas, and T. Wlodarczyk, *SpECTRE* (2020).
- [53] K. Mitman *et al.*, Fixing the BMS frame of numerical relativity waveforms, *Phys. Rev. D* **104**, 024051 (2021), [arXiv:2105.02300 \[gr-qc\]](#).
- [54] K. Mitman *et al.*, Fixing the BMS Frame of Numerical Relativity Waveforms with BMS Charges, [arXiv:2208.04356 \[gr-qc\]](#).
- [55] M. Boyle, D. Iozzo, and L. C. Stein, *moble/scri: v1.2* (2020).
- [56] M. Boyle, Angular velocity of gravitational radiation from precessing binaries and the corotating frame, *Phys. Rev. D* **87**, 104006 (2013), [arXiv:1302.2919 \[gr-qc\]](#).
- [57] M. Boyle, L. E. Kidder, S. Ossokine, and H. P. Pfeiffer, Gravitational-wave modes from precessing black-hole binaries, [arXiv:1409.4431 \[gr-qc\]](#).
- [58] M. Boyle, Transformations of asymptotic gravitational-wave data, *Phys. Rev. D* **93**, 084031 (2016), [arXiv:1509.00862 \[gr-qc\]](#).
- [59] P. Virtanen, R. Gommers, T. E. Oliphant, M. Haberland, T. Reddy, D. Cournapeau, E. Burovski, P. Peterson, W. Weckesser, J. Bright, S. J. van der Walt, M. Brett, J. Wilson, K. J. Millman, N. Mayorov, A. R. J. Nelson, E. Jones, R. Kern, E. Larson, C. J. Carey, Í. Polat, Y. Feng, E. W. Moore, J. VanderPlas, D. Laxalde, J. Perktold, R. Cimrman, I. Henriksen, E. A. Quintero, C. R. Harris, A. M. Archibald, A. H. Ribeiro, F. Pedregosa, P. van Mulbregt, and SciPy 1.0 Contributors, SciPy 1.0: Fundamental Algorithms for Scientific Computing in Python, *Nature Methods* **17**, 261 (2020).
- [60] L. C. Stein, qnm: A Python package for calculating Kerr quasinormal modes, separation constants, and spherical-spheroidal mixing coefficients, *J. Open Source Softw.* **4**, 1683 (2019), [arXiv:1908.10377 \[gr-qc\]](#).
- [61] Besides the amplitudes, we can also check the consistency of the phases of the quadratic (4, 4) QNM and the linear (2, 2, 0) QNM. We find that the phase of $A_{(4,4)}^{(2,2,0) \times (2,2,0)} / A_{(2,2,0)}^2$ is always within 0.4 radians of 0, for each simulation, for start times in the range $u_0 \in [15M, 30M]$.
- [62] S. Borhanian, K. G. Arun, H. P. Pfeiffer, and B. S. Sathyaprakash, Comparison of post-Newtonian mode amplitudes with numerical relativity simulations of binary black holes, *Class. Quant. Grav.* **37**, 065006 (2020), [arXiv:1901.08516 \[gr-qc\]](#).
- [63] We also find the peak amplitude $A_{(4,4,1)}$ to be comparable or sometimes larger than $A_{(4,4)}^{(2,2,0) \times (2,2,0)}$ (see bottom panel of Fig. 3) but, since $\text{Im}[M\omega_{(4,4,1)}] = -0.25$, this (4, 4, 1) mode decays fast enough that it will be comparable or smaller than the quadratic (4, 4) mode after $u = 10M$.
- [64] The numerical error for the other simulations tends to be worse since they were not run with as fine of a resolution, but the errors are nonetheless comparable to that of SXS:BBH:0305.
- [65] Except for a few simulations at early times $u_0 \lesssim 15M$, for which the linear model can have a marginally better mismatch.
- [66] L. Sberna, P. Bosch, W. E. East, S. R. Green, and L. Lehner, Nonlinear effects in the black hole ringdown: Absorption-induced mode excitation, *Phys. Rev. D* **105**, 064046 (2022), [arXiv:2112.11168 \[gr-qc\]](#).
- [67] M. H.-Y. Cheung *et al.*, Nonlinear effects in black hole ringdown, In prep..
- [68] E. W. Leaver, Spectral decomposition of the perturbation response of the Schwarzschild geometry, *Phys. Rev. D* **34**, 384 (1986).
- [69] K. Mitman, J. Moxon, M. A. Scheel, S. A. Teukolsky, M. Boyle, N. Deppe, L. E. Kidder, and W. Thrope, Computation of displacement and spin gravitational memory in numerical relativity, *Phys. Rev. D* **102**, 104007 (2020), [arXiv:2007.11562 \[gr-qc\]](#).